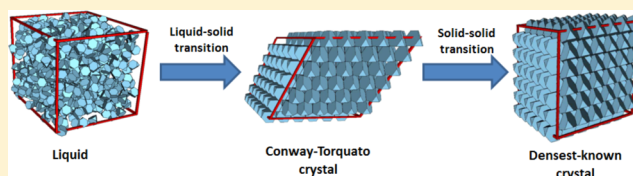


Equilibrium Phase Behavior and Maximally Random Jammed State of Truncated Tetrahedra

Duyu Chen,^{†,‡} Yang Jiao,[#] and Salvatore Torquato^{*,†,‡,§,||,⊥}[†]Department of Chemistry, Princeton University, Princeton, New Jersey 08544, United States[‡]Physical Science in Oncology Center, Princeton University, Princeton, New Jersey 08544, United States[#]Materials Science and Engineering, Arizona State University, Tempe, Arizona 85287, United States[§]Department of Physics, Princeton University, Princeton, New Jersey 08544, United States^{||}Program in Applied and Computational Mathematics, Princeton University, Princeton, New Jersey 08544, United States[⊥]Princeton Institute of the Science and Technology of Materials, Princeton University, Princeton, New Jersey 08544, United States

ABSTRACT: Numerous recent investigations have been devoted to the determination of the equilibrium phase behavior and packing characteristics of hard nonspherical particles, including ellipsoids, superballs, and polyhedra, to name but just a few shapes. Systems of hard nonspherical particles exhibit a variety of stable phases with different degrees of translational and orientational order, including isotropic liquid, solid crystal, rotator and a variety of liquid crystal phases. In this paper, we employ a Monte Carlo implementation of the adaptive-shrinking-cell (ASC) numerical scheme and free-energy calculations to ascertain with high precision the equilibrium phase behavior of systems of congruent Archimedean truncated tetrahedra over the entire range of possible densities up to the maximal nearly space-filling density. In particular, we find that the system undergoes two first-order phase transitions as the density increases: first a liquid–solid transition and then a solid–solid transition. The isotropic liquid phase coexists with the Conway–Torquato (CT) crystal phase at intermediate densities, verifying the result of a previous qualitative study [*J. Chem. Phys.* **2011**, *135*, 151101]. The freezing- and melting-point packing fractions for this transition are respectively $\phi_F = 0.496 \pm 0.006$ and $\phi_M = 0.591 \pm 0.005$. At higher densities, we find that the CT phase undergoes another first-order phase transition to one associated with the densest-known crystal, with coexistence densities in the range $\phi \in [0.780 \pm 0.002, 0.802 \pm 0.003]$. We find no evidence for stable rotator (or plastic) or nematic phases. We also generate the maximally random jammed (MRJ) packings of truncated tetrahedra, which may be regarded to be the glassy end state of a rapid compression of the liquid. Specifically, we systematically study the structural characteristics of the MRJ packings, including the centroidal pair correlation function, structure factor and orientational pair correlation function. We find that such MRJ packings are hyperuniform with an average packing fraction of 0.770, which is considerably larger than the corresponding value for identical spheres (≈ 0.64). We conclude with some simple observations concerning what types of phase transitions might be expected in general hard-particle systems based on the particle shape and which would be good glass formers.



I. INTRODUCTION

Hard-particle systems have served as useful models of low-temperature states of matter, including liquids,¹ crystals,² glasses,^{2,3} granular media,^{4,5} heterogeneous materials,⁴ and powders.⁶ Understanding the equilibrium and nonequilibrium properties of hard particle systems is of great interest. This is reflected by the numerous studies devoted to these topics for nonspherical particles that span a wide range of shapes, including ellipsoids, superballs, and polyhedra.^{1,7–19} Nanoparticles and colloidal particles of various shapes can now be routinely synthesized in the laboratory.^{20–23}

In general, a packing is defined as a large collection of nonoverlapping solid objects (particles) in d -dimensional Euclidean space \mathbb{R}^d . The associated packing fraction (or density) ϕ is defined as the fraction of space \mathbb{R}^d covered by the particles. The densest packing of a specific particle shape, which is usually achieved by an ordered arrangement depending

on the particle symmetry,^{17,18} is the thermodynamic stable phase of that shape in the infinite-pressure limit,²⁵ and thus provides the starting point to determine the entire high-density phase behavior of the system. On the other hand, the maximally random jammed (MRJ) state of packing can be considered to be a prototypical glass.^{24,25} Roughly speaking, MRJ packings can be obtained by compressing liquid configurations at the largest possible rate such that the packing is strictly jammed (i.e., mechanically stable).²⁵

The hard-sphere model in \mathbb{R}^3 has a venerable history.^{1,4,25–33} It is well-known from numerical simulations that such a system exhibits a first-order liquid-crystal phase transition as the

Special Issue: James L. Skinner Festschrift

Received: January 28, 2014

Revised: March 11, 2014

Published: April 9, 2014

density increases along the liquid branch. The associated freezing- and melting-point packing fractions have been determined to be around 0.49 and 0.55, respectively, by both pressure and free-energy calculations.^{1,25} At the maximal density, free-energy calculations have been used to demonstrate that the face-centered cubic crystal (FCC) is very slightly more stable than the hexagonal close-packed crystal.^{28,30,31} Upon rapid compression from a liquid configuration, the system falls out of equilibrium and follows a metastable branch, whose end state is presumably the MRJ state in the infinite-volume limit.^{25,29} The aforementioned equilibrium and nonequilibrium properties of the hard-sphere system are schematically illustrated in Figure 1.

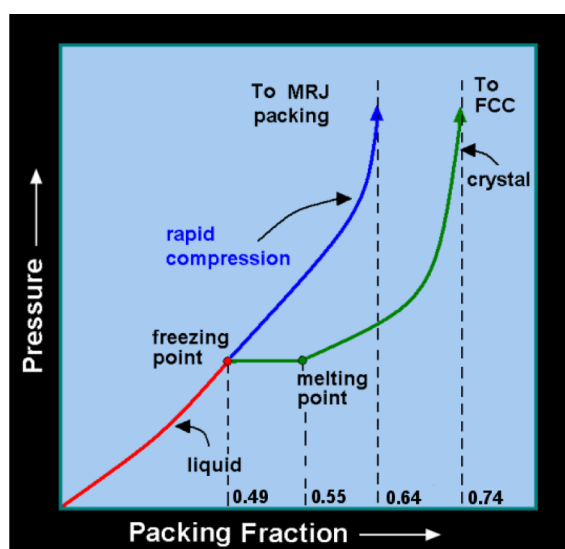


Figure 1. Schematic plot for the pressure of the hard-sphere system as a function of packing fraction along the stable liquid and crystal branches, and along a metastable branch ending at the MRJ state in the infinite-volume limit. This figure is adapted from ref 25.

Since nonspherical particles have both translational and rotational degrees of freedom, they usually have a richer phase diagram than spheres, i.e., the former can possess different degrees of translational and orientational order. For example, a rotator (or plastic) phase is one in which particles possess translational order but can rotate freely.^{34–36} A nematic phase is one in which the particles are aligned (i.e., with orientational order) while the system lacks any long-range translational order.^{37,38} A smectic phase is one in which particles have ordered orientations and possess translational order in one direction.³⁹ The types of phases formed by hard nonspherical particles are influenced by many factors. It is well-known that entropy plays a principal role in determining the phase behavior of hard-particle systems. For example, spheroids (ellipsoids of revolution) with needle-like shapes exhibit a liquid-nematic phase transition at low densities.³⁷ While more recent studies^{7,8} have also revealed that spheroids with shapes closer to spheres exhibit a liquid-rotator crystal phase transition at intermediate densities. It has been demonstrated that the local curvature of the particle shape contributes to the stabilization of rotator phases by studies of superballs at intermediate densities.^{9,40} Gantapara et al.¹² showed that the phase diagram of truncated cubes exhibits a rich diversity in crystal structures that depend sensitively on the amount of truncation. When the interactions are dominated by hard-particle-like repulsions, such as in

certain polymer systems, the role of entropy is significant as well.⁴¹

One aim of this paper is to determine systematically the equilibrium phase behavior of the Archimedean truncated tetrahedra for the entire density range. An Archimedean truncated tetrahedron (henceforth often called a truncated tetrahedron for simplicity) is obtained by truncating the corners of a regular tetrahedron with edge length that is one-third of the edge length of the original tetrahedron, and it therefore has four regular triangular faces and four hexagonal faces. It is of particular interest because it is the only nonchiral Archimedean solid without central symmetry and, as we will discuss, packings of truncated tetrahedra can nearly fill all of the space. Some geometrical properties of the truncated tetrahedron, including the inradius r_{in} , circumradius r_{out} , asphericity $\gamma \equiv r_{out}/r_{in}$, radius of mean curvature \bar{R} ,⁴² surface area S , volume v , and scaled exclusion volume v_{ex}/v ,⁴² are summarized in Table 1.

Table 1. Some Geometrical Properties of the Archimedean Truncated Tetrahedron with Side Length a

inradius, r_{in}	$(6a)^{1/2}/4$
circumradius, r_{out}	$(22a)^{1/2}/4$
asphericity, γ	$\sqrt{(33/3)}$
radius of mean curvature, \bar{R}	$(9/4\pi)\cos^{-1}(1/3)a$
surface area, S	$7(3a^2)^{1/2}$
volume, v	$(23/12)(2a^3)^{1/2}$
scaled exclusion volume, v_{ex}/v	$2 + (378/23\pi)(3/2)^{1/2} \cos^{-1}(1/3)$

Jiao and Torquato¹⁰ have recently analytically constructed the densest known packing of such polyhedra with $\phi = 207/208 = 0.995192\dots$. Given that this packing fraction is nearly equal to unity and truncated tetrahedra cannot tile three-dimensional Euclidean space \mathbb{R}^3 , this densest known packing is likely the densest packing for such solids. In the same paper, the equilibrium melting properties of truncated tetrahedra were also qualitatively studied by simply monitoring the structural changes upon decompression from the densest known packing. They found that the system apparently undergoes a transition to another crystal phase, namely the one associated with the packing of truncated tetrahedra discovered by Conway and Torquato⁴³ (henceforth referred to as “CT crystal”) as well. Figure 2 shows a portion of the CT packing and the densest known packing. However, only free-energy calculations can yield quantitatively accurate information about the phase behavior of truncated tetrahedra over the entire range of densities.

In the present work, we employ a Monte Carlo implementation of the adaptive-shrinking-cell (ASC) numerical scheme^{17,18} and free-energy calculations¹ to investigate with high precision the equilibrium phase behavior of truncated tetrahedra and to verify whether the types of phases found in ref 10 are indeed thermodynamically stable. Consistent with the findings of ref 10, we find that the system undergoes two first-order phase transitions as the density increases: first a liquid–solid transition and then a solid–solid transition. The isotropic liquid phase coexists with the Conway–Torquato (CT) crystal phase with densities in the range $\phi \in [0.496 \pm 0.006, 0.591 \pm 0.005]$. At higher densities, the CT phase coexists with the one associated with the densest-known crystal with densities in the range $\phi \in [0.780 \pm 0.002, 0.802 \pm 0.003]$. We find no evidence for stable rotator or nematic phases. Moreover, we also generate maximally random jammed packings of truncated

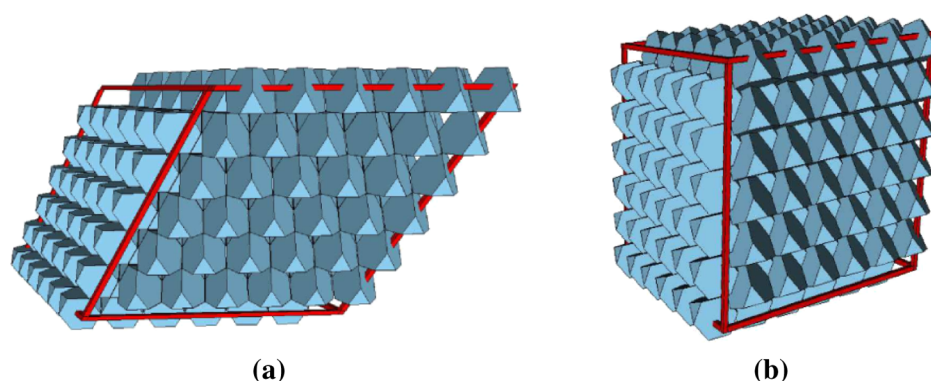


Figure 2. (a) Portion of the CT crystal. (b) Portion of the densest known crystal.

tetrahedra using ASC simulations with a sufficient large compression rate and study their characteristics, including the packing fraction, centroidal pair correlation function, structure factor and orientational correlation function. We find that the MRJ packings are hyperuniform⁴⁴ (see section V for definitions and details). In closing, we explain why truncated tetrahedra are expected to have the two types of first-order phase transitions reported here.

The rest of the paper is organized as follows: In section II, we discuss the simulation methods used in studying the phase behavior of truncated tetrahedra. In section III, we discuss the structural descriptors used to characterize equilibrium and MRJ packings of truncated tetrahedra. In section IV, we study the equilibrium phase behavior of truncated tetrahedra using ASC simulations and free-energy calculations. In section V, we generate and characterize MRJ packings of truncated tetrahedra. In section VI, we provide concluding remarks and make some simple observations concerning what types of phase transitions might be expected in general hard-particle systems based on the particle shape.

II. SIMULATION PROCEDURES FOR PHASE BEHAVIOR

A. Adaptive-Shrinking-Cell Monte Carlo Method. The adaptive-shrinking-cell (ASC) Monte Carlo method is employed to equilibrate hard truncated tetrahedra at different packing fractions. While we sketch the procedure here, the reader is referred to ref 18 for additional details. Along the liquid branch, initially a system at each packing fraction is generated by compressing dilute disordered particle configurations with $\phi < 0.1$ in a simulation box subject to periodic boundary conditions. Along the crystal branch, initially a system at each packing fraction is generated by dilating the densest crystal of the particles in a simulation box subject to periodic boundary conditions. Our ASC scheme is capable of shrinking the simulation box, but we do not employ that feature for the determination of the phase behavior (just use it for the generation of MRJ states, as described in section V). The initial systems at fixed densities are equilibrated by particle trial moves and volume-preserving shear deformations of the simulation box. Specifically, for a fixed simulation box, each particle is sequentially randomly displaced and rotated by small amounts. A trial move is rejected if it results in overlap between a pair of particles and is accepted otherwise. The *separation axis theorem* (SAT)⁴⁵ is used to check overlaps. After a prescribed number of trial-move cycles, the boundary of the periodic simulation box (fundamental cell) is allowed to deform by specified small amount. Such a boundary move is accepted if no overlaps

between any pair of particles in the system occur and is rejected otherwise. The boundary deformation is represented by a symmetric strain tensor, whose trace (i.e., the sum of the diagonal components) corresponds to the volume change (i.e., compression or expansion) of the fundamental cell, and the off-diagonal components correspond to the shape change (i.e., deformation) of the fundamental cell. The equilibrium pressure is obtained as discussed in the ensuing section.

B. Pressure Calculation. The equilibrium pressure of the truncated-tetrahedron system in our NVT simulation is computed from the distribution of interparticle gaps. Following ref 46, the scaled pressure Z is given by

$$Z \equiv \frac{p}{\rho k_B T} = 1 + \frac{\phi \alpha}{2} \quad (1)$$

where $\rho = N/V$ is the number density of the system, T is the temperature, and k_B is the Boltzmann's constant. The parameter α depends on the particle shape and is computed from the following relation:

$$\ln P_1(\Delta\phi) = \ln \alpha - \alpha \Delta\phi \quad (2)$$

where $P_1(\Delta\phi)$ is the probability that a given particle first overlaps with another particle if the packing fraction of the system is increased by $\Delta\phi$, regardless of other overlapping pairs of particles.

In practice, one just needs to compute for each particle the minimal compression (i.e., change of volume) leading to overlap between it and its nearest neighbor. This process is repeated for every particle in the system and a histogram of the distribution of minimal interparticle gaps is then obtained.

C. Free Energy Calculations. *Free Energy Calculations of the Liquid Phase.* To compute the free energy of the liquid phase, we first use pressure calculations discussed in section II.A to obtain the associated dimensionless equation of state (EOS) for the scaled pressure, i.e., $Z = p/(\rho k_B T)$. Then we integrate the EOS from a low-density reference state with packing fraction ϕ_0 to a specific ϕ to get the associated Helmholtz free energy,¹¹ i.e.

$$\frac{A(\phi)}{Nk_B T} = \frac{A(\phi_0)}{Nk_B T} + \int_{\phi_0}^{\phi} \frac{p(\phi')v}{k_B T \phi'^2} d\phi' \quad (3)$$

where

$$A(\phi_0)/(Nk_B T) = \mu(\phi_0)/(k_B T) - p(\phi_0)v/(k_B T \phi_0) \quad (4)$$

and v is the volume of a particle and $\mu(\phi_0)$ the chemical potential at packing fraction ϕ_0 , which is calculated by Widom's

particle insertion method.⁴⁷ In this paper, we use a reference system at $\phi_0 = 0.10$ for liquid-phase free energy calculations.

Free Energy Calculations of a Solid Phase. To compute the free energy of a solid phase, we employ the standard NVT Einstein crystal method.^{1,9,11,48} Specifically, we construct a reversible path between the actual hard-particle crystal and an ideal Einstein crystal, which allows us to calculate the free-energy difference between these two systems. Since the free energy of the ideal Einstein crystal is known analytically, we can thus obtain the absolute value of the free energy for the hard-particle crystal, i.e.

$$\frac{A(N, V, T)}{k_B T} = \frac{A_E(N, V, T)}{k_B T} - \int_0^{\lambda_{\max}} d\lambda \left\langle \frac{\partial U_E(\lambda)}{\partial \lambda} \right\rangle \quad (5)$$

where $\langle \dots \rangle$ denotes ensemble average of systems with coupling potential U_E and λ_{\max} is the maximum coupling constant that is sufficiently strong to suppress particle collisions. When $\lambda = \lambda_{\max}$, the system behaves like an ideal Einstein crystal. When $\lambda = 0$, there is no coupling potential and the system behaves as the real crystal under consideration. The free energy of the ideal Einstein crystal $A_E(N, V, T)$ is given by

$$\begin{aligned} \frac{A_E(N, V, T)}{k_B T} = & -\frac{3(N-1)}{2} \ln \left(\frac{\pi k_B T}{\lambda_{\max}} \right) + N \ln \left(\frac{\Lambda_t^3 \Lambda_r}{\sigma^4} \right) \\ & + \ln \left(\frac{\sigma^3}{VN^{1/2}} \right) - N \ln \left\{ \frac{1}{8\pi^2} \int d\theta \, d\phi \, d\chi \right. \\ & \left. \sin \theta \exp \left[-\frac{\lambda_{\max}}{k_B T} (\sin^2 \psi_a + \sin^2 \psi_b) \right] \right\} \end{aligned} \quad (6)$$

where Λ_t and Λ_r are the translational and rotational thermal de Broglie wavelengths, respectively, and both are set to 1 in our simulations; $\sigma = 1/v^{1/3}$ is the characteristic length of the particle with volume v ; θ , ϕ and χ are the Euler angles⁴⁹ defining the orientation of the particle with respect to the reference orientation in the reference lattice; ψ_a and ψ_b are the minimal angles formed by the two reference vectors \mathbf{a} , \mathbf{b} and the characteristic vectors of a particle defining its orientation. The potential $U_E(\lambda)$ characterizes the coupling between the hard particles to their reference lattice sites and reference orientations,^{9,50} i.e.,

$$U_E(\lambda) = \lambda \sum_{i=1}^N [(\mathbf{r}_i - \mathbf{r}_{i0})^2 / \sigma^2 + (\sin^2 \psi_{ia} + \sin^2 \psi_{ib})] \quad (7)$$

where $\mathbf{r}_i - \mathbf{r}_{i0}$ is the displacement of particle i with respect to its reference lattice site.

Validation of Free Energy Calculation. To validate our implementation of the free energy calculations, we have calculated the free energy of hard regular octahedra within intermediate density ranges, where it has been previously shown that there is a first-order liquid to Minkowski crystal⁵¹ phase transition.^{9,12} Our results are shown in Figure 3. On the basis of our free energy calculations, we estimate the freezing- and melting-point packing fractions of hard octahedra to be 0.489 ± 0.004 and 0.582 ± 0.008 , respectively, which agree well with previously reported values in the literature.^{9,12}

III. STRUCTURAL DESCRIPTORS

In this section, we present a number of structural descriptors that quantitatively characterize various packing structures of

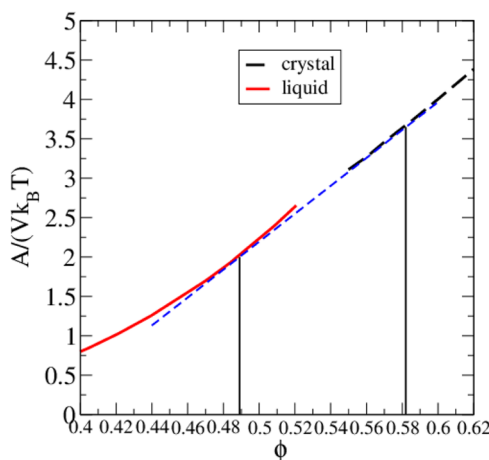


Figure 3. Reduced Helmholtz free energy per unit volume $A/(Vk_B T)$ as a function of packing fraction ϕ for hard octahedra. The liquid phase is found to coexist with the Minkowski crystal. The freezing- and melting-point packing fractions are estimated to be 0.489 ± 0.004 and 0.582 ± 0.008 , respectively.

truncated tetrahedra that are associated with the equilibrium and nonequilibrium phases of the system. In addition, we briefly review the “hyperuniformity” concept and its quantification, which appears to be a universal structural characteristic of general maximally random jammed packings.

A. Orientational Pair Correlation Function. The emergence of orientational order in a MC simulations is usually a strong indication of a possible first-order phase transition. To quantify the orientational order in the system of truncated tetrahedra at different densities, we use an orientational pair correlation function, which we define as

$$g_{\text{orient}}(r) = \frac{\sum_{i=1}^N \sum_{j \neq i}^N \delta(r - r_{ij}) (\sin^2 \alpha_{ij}^{F_1} + \sin^2 \alpha_{ij}^{F_2}) / 2}{\sum_{i=1}^N \sum_{j \neq i}^N \delta(r - r_{ij})} \quad (8)$$

where $\alpha_{ij}^{F_1}$ is the minimum angle formed by any of the characteristic vectors associated with truncated tetrahedron i and any of the characteristic vectors associated with truncated tetrahedron j , and $\alpha_{ij}^{F_2}$ is the second minimum besides $\alpha_{ij}^{F_1}$ ($\alpha_{ij}^{F_1} \leq \alpha_{ij}^{F_2}$). We define a characteristic vector associated with a truncated tetrahedron as the unit vector pointing from the particle centroid to the center of one of the four hexagonal faces of a truncated tetrahedron. The superscript F_1 denotes such pair of characteristic vectors passing through the hexagonal face centers that minimizes the angle between them, and F_2 denotes the next pair that minimizes the angle besides the pair associated with F_1 . The orientational pair correlation function will be employed to suggest possible stable phases for subsequent free energy calculations.

B. Structure Factor and Centroidal Pair Correlation Function. The ensemble-averaged structure factor of infinite point configurations in d -dimensional Euclidean space at number density ρ is defined via

$$S(\mathbf{k}) = 1 + \rho \tilde{h}(\mathbf{k}) \quad (9)$$

where $\tilde{h}(\mathbf{k})$ is the Fourier transform of the total correlation function $h(\mathbf{r}) = g_2(\mathbf{r}) - 1$ and $g_2(\mathbf{r})$ is the centroidal pair correlation function of the system. Note that definition 9 implies that the forward scattering contribution to the diffraction pattern is omitted. For statistically homogeneous

and isotropic systems, the focus of this paper, g_2 depends on the radial distance $r \equiv |\mathbf{r}|$ between the points as well as the number density ρ .

For computational purposes, the structure factor $S(\mathbf{k})$ for a given finite point configuration can be obtained directly from the positions of the points \mathbf{r}_j ,⁵³ i.e.

$$S(\mathbf{k}) = \frac{1}{N} \left| \sum_{j=1}^N \exp(i\mathbf{k} \cdot \mathbf{r}_j) \right|^2 \quad (\mathbf{k} \neq \mathbf{0}) \quad (10)$$

where N is the total number points in the system (under periodic boundary conditions) and \mathbf{k} is the wave vector. Note that the forward scattering contribution ($\mathbf{k} = \mathbf{0}$) in equation 10 is omitted, which makes relation 10 completely consistent with the definition 9 in the ergodic infinite-system limit. For statistically homogeneous and isotropic systems, the focus of this paper, the structure factor $S(k)$ only depends on the magnitude of the scalar wavenumber $k = |\mathbf{k}| = 2\pi n/L$, where $n = 0, 1, 2, \dots$, and L is the linear size of the system.

C. Hyperuniform Systems. The small- k behavior of the structure factor $S(k)$ encodes information about large-scale spatial correlations in the system and in the limit $k \rightarrow 0$ determines whether the system is hyperuniform. Specifically, an infinite point configuration in d -dimensional Euclidean space is *hyperuniform* if

$$\lim_{k \rightarrow 0} S(k) = 0 \quad (11)$$

which implies that the infinite-wavelength density fluctuations of the system (when appropriately scaled) vanish.⁴⁴

A hyperuniform point configuration has the property that the variance in the number of points in an observation window Ω grows more slowly than the volume of that window.⁴⁴ In the case of a spherical observation window of radius R , this definition implies that the local number variance $\sigma^2(R)$ grows more slowly than R^d in d dimensions. The local number variance of a statistically homogeneous point configuration in a spherical observation window is given exactly by

$$\sigma^2(R) = \rho v(R) \left[1 + \rho \int_{\mathbb{R}^d} h(\mathbf{r}) \alpha(\mathbf{r}; R) d\mathbf{r} \right] \quad (12)$$

where $v(R)$ is the volume of a spherical window of radius R and $\alpha(\mathbf{r}; R)$ is the *scaled intersection volume*, i.e., the intersection volume of two spheres of radius R separated by a distance r divided by the volume of a sphere $v(R)$.

It has been shown that the number variance in eq 12, under certain conditions, admits the following asymptotic scaling:⁴⁴

$$\sigma^2(R) = 2^d \phi \left\{ A \left(\frac{R}{D} \right)^d + B \left(\frac{R}{D} \right)^{d-1} + o \left[\left(\frac{R}{D} \right)^{d-1} \right] \right\} \quad (13)$$

where

$$A = 1 + \rho \int_{\mathbb{R}^d} h(\mathbf{r}) d\mathbf{r} = \lim_{\|\mathbf{k}\| \rightarrow 0} S(\mathbf{k}) \quad (14)$$

D is a characteristic microscopic length associated with the point configuration (e.g., the average nearest-neighbor distance between the points) and $o(x)$ denotes all terms of order less than x . Clearly, when the coefficient $A = 0$, i.e., $\lim_{k \rightarrow 0} S(k) = 0$ satisfies the requirements for hyperuniformity. The relation in 14 then implies that hyperuniform point patterns do not possess infinite-wavelength density fluctuations (when appropriately scaled) and hence from 13 the number variance scales

as the surface area of the window for large R , i.e., $\sigma^2(R) \sim R^{d-1}$ in the large- R limit. Equations 13 and 14 are valid for all periodic point patterns (including perfect lattices), quasicrystals, and disordered systems in which the pair correlation function g_2 decays to unity exponentially fast.⁴⁴ The degree to which large-scale density fluctuations are suppressed enables one to rank order crystals, quasicrystals and special disordered systems.^{44,53}

Disordered hyperuniform structures can be regarded as new states of disordered matter in that they behave more like crystals or quasicrystals in the manner in which they suppress density fluctuations on large length scales, and yet are also like liquids and glasses in that they are statistically isotropic structures with no Bragg peaks. Thus, disordered hyperuniform materials can be regarded to possess a “hidden order” that is not apparent on short length scales and are endowed with novel physical properties. Such states of matter can be arrived at via both equilibrium and nonequilibrium routes and include fermionic ground states,⁵⁴ classical disordered ground states,⁵⁵ and MRJ particle packings.^{15,56–59} Disordered hyperuniform dielectric network materials have been shown to possess large and complete photonic band gaps.⁶⁰ More recently, it has been demonstrated that this exotic state of matter arises in the photoreceptor patterns in avian retinas.⁶¹

For disordered hyperuniform systems with a total correlation function $h(r)$ that does not decay to zero exponentially fast, other dependencies of the number variance on R may be observed. More generally, for any reciprocal power law,

$$S(k) \sim k^\alpha (k \rightarrow 0) \quad (15)$$

or, equivalently,

$$h(r) \sim -\frac{1}{r^{d+\alpha}} (r \rightarrow +\infty) \quad (16)$$

one can observe a number of different kinds of dependencies of the asymptotic number variance σ^2 on the window radius R for $R \rightarrow \infty$:^{44,53,57}

$$\sigma^2(R) \sim \begin{cases} R^{d-1} \ln R, & \alpha = 1 \\ R^{d-\alpha}, & \alpha < 1 \\ R^{d-1}, & \alpha > 1 \end{cases} \quad (17)$$

Note that in all cases, the number variance of a hyperuniform point pattern grows more slowly than R^d .

IV. EQUILIBRIUM PHASE BEHAVIOR OF TRUNCATED TETRAHEDRA

To explore the possible phases arising in the system of hard truncated tetrahedra, we first carry out ASC simulations and quantify the orientational order in the system. Specifically, we compute the orientational pair correlation function [as defined in eq 8] for equilibrated systems with $N = 686$ particles at different densities. As shown in Figure 4, below $\phi \approx 0.53$, there is no long-range orientational correlation in the system, while around $\phi = 0.57$ long-range orientational correlation begins to emerge. Together with the centroidal pair correlation function g_2 characterizing the translational order reported previously,¹⁰ we find that the orientational order and translational order arise almost simultaneously during a possible first-phase liquid–solid phase transition. These results strongly suggest that the truncated tetrahedron system possesses neither stable nematic nor rotator phases.

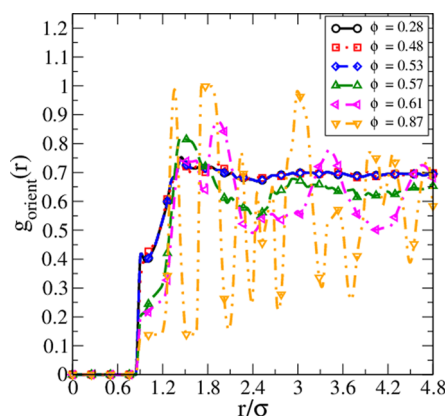


Figure 4. Orientational pair correlation function $g_{\text{orient}}(r)$ as a function of the dimensionless distance r/σ (where $\sigma = v^{1/3}$) for equilibrated systems of hard truncated tetrahedra at different packing fractions $\phi = 0.28, 0.48, 0.53, 0.57, 0.61$, and 0.87 . Below $\phi \approx 0.53$, there is no long-range orientational correlation in the system, while around $\phi = 0.57$ long-range orientational correlation arises.

A. First-Order Liquid–Solid Phase Transition of Truncated Tetrahedra. We employ pressure and free energy calculations to determine precisely the freezing- and melting-point packing fractions for hard truncated tetrahedra. Specifically, we calculate the reduced pressure, i.e., $pv/(k_B T)$ vs ϕ for the liquid branch, liquid–solid phase transition region, and the crystal branch, where v is the volume of a truncated tetrahedron. A periodic simulation box containing $N = 686$ hard truncated tetrahedra is employed. A system at each density is initially generated by dilating the fundamental cell of the densest crystal of the particles, which is then equilibrated. At each density, at least 500000 MC trial moves per particle and 5000 trial volume-preserving shear deformations of the fundamental cell are applied to equilibrate the system. Then the pressure of the equilibrated system is collected. As shown in Figure 5, the reduced pressure $pv/(\rho k_B T)$ increases smoothly with ϕ along the equilibrium liquid branch up to a density $\phi \approx 0.49 \pm 0.01$. Within the density range between $\phi \approx 0.49 \pm 0.01$ and $\phi \approx 0.59 \pm 0.01$, the trend of the reduced pressure exhibits discontinuities, suggesting that metastable states exist in this region. (These coexistence densities will be determined more precisely by free energy calculations below.) Beyond $\phi \approx 0.59 \pm 0.01$, the trend becomes smooth again, suggesting that the system enters an equilibrium solid branch.

For the liquid branch, we compare the fit of our data for the dimensionless pressure $Z = p/(\rho k_B T)$ to the Boublík's analytical approximation for the EOS⁶² for convex hard particles, which is given by

$$Z = \frac{1}{1 - \phi} + \frac{3A\phi}{(1 - \phi)^2} + \frac{3A^2\phi^2 - A(6A - S)\phi^3}{(1 - \phi)^3} \quad (18)$$

where $A = S\bar{R}/3v$ is the nonsphericity parameter (S , \bar{R} , v are the surface area, radius of mean curvature, volume of a single particle, respectively). As shown in Figure 6, the Boublík's EOS appreciably underestimates the simulation data, which indicates the need for an improved analytical approximation for the EOS.

To precisely locate the freezing- and melting-point packing fractions associated with this first-order transition, we calculate the free energies for the liquid and CT crystal phase at different densities. For the liquid phase, a periodic simulation box

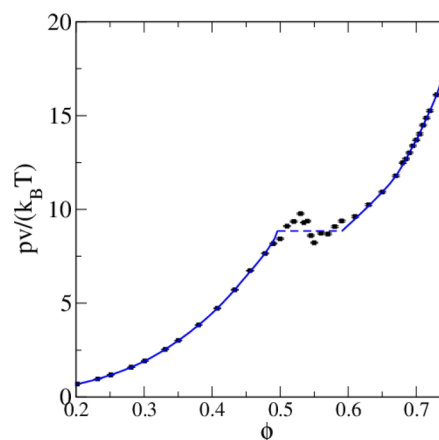


Figure 5. Reduced pressure $pv/(k_B T)$ as a function of packing fraction ϕ for the liquid branch (below $\phi \approx 0.49 \pm 0.01$), liquid–solid phase transition region (between $\phi \approx 0.49 \pm 0.01$ and $\phi \approx 0.59 \pm 0.01$) and the crystal branch (above $\phi \approx 0.59 \pm 0.01$) of hard truncated tetrahedra, where v is the volume of a truncated tetrahedron. The square dots are the actual simulation data and the solid curves are the fits of the data for the liquid and crystal branches, respectively. The horizontal dash line denotes the coexistence region between the liquid and the CT crystal, which is determined by subsequent free energy calculations.

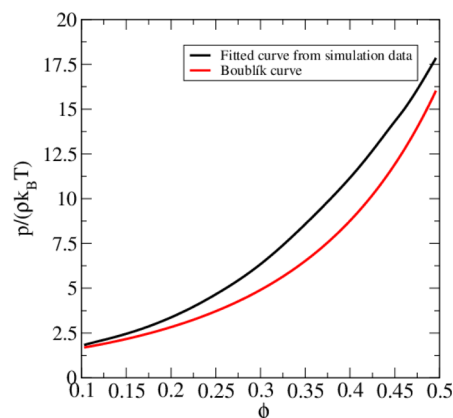


Figure 6. $Z = p/(\rho k_B T)$ as a function of packing fraction ϕ for the liquid branch by Boublík's expression and simulation data, respectively. Note that the two curves diverge appreciably.

containing $N = 686$ hard truncated tetrahedra is employed. At each density, at least 500000 MC trial moves per particle and 5000 trial volume-preserving shear deformations of the fundamental cell are applied to equilibrate the system. For the CT crystal phase, to eliminate finite-size effects, we use four different system sizes ($N = 432$, $N = 1024$, $N = 1458$, and $N = 2000$) and extrapolate the corresponding free energies to obtain the infinite-size limit.⁶³ To suppress particle collisions, λ_{max} in eq 5 is chosen to be 2000. For each system, 40000 MC cycles (i.e., a sequential trial move of each particle) are used to equilibrate the system and another 40000 cycles are used to compute the ensemble-averaged value of $U(\lambda)$ at each integration point in eq 5.

After the Helmholtz free energy per unit volume $A/(Nk_B T)$ as a function of ϕ for different phases are obtained, we employ a common tangent construction, as shown in Figure 7, to find precisely the coexistence densities.⁹ We find that the freezing-

and melting-point packing fractions are respectively given by $\phi = 0.496 \pm 0.006$ and $\phi = 0.591 \pm 0.005$.

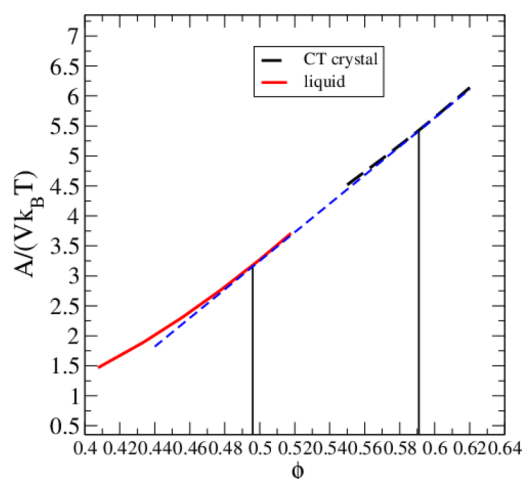


Figure 7. Reduced Helmholtz free energy per unit volume $A/(Vk_B T)$ as a function of packing fraction ϕ in the vicinity of the liquid-CT crystal coexistence region of hard truncated tetrahedra. The freezing- and melting-point packing fractions of hard truncated tetrahedra are estimated to be $\phi = 0.496 \pm 0.006$ and $\phi = 0.591 \pm 0.005$, respectively.

B. First-Order Solid–Solid Phase Transition of Truncated Tetrahedra. Jiao and Torquato suggested that there is a solid–solid phase transition between the CT crystal and the densest known crystal at high densities by monitoring structural changes upon decompression from the densest crystal.¹⁰ However, the nature of this transition and the exact transition densities were not determined in their study. Here we employ pressure and free-energy calculations to investigate this putative solid–solid phase transition.

Specifically, we calculate the reduced pressure $pv/(k_B T)$ as a function of ϕ for $\phi \in [0.76, 0.85]$. A periodic simulation box containing $N = 686$ hard truncated tetrahedra is employed. At each density, at least 500000 MC trial moves per particle and 5000 trial volume-preserving shear deformations of the fundamental cell are applied to equilibrate the system. The pressure of the equilibrated system is then collected. As shown in Figure 8, between $\phi \approx 0.775 \pm 0.005$ and $\phi \approx 0.800 \pm 0.002$, the trend of the reduced pressure $pv/(k_B T)$ versus ϕ exhibits a weak discontinuity, suggesting a possible first-order solid–solid phase transition, which is consistent with the qualitative study of Jiao and Torquato¹⁰ in which structural changes upon decompression were monitored.

To precisely locate the coexistence densities associated with this transition, we calculate the free energy for the CT crystal and densest known crystal at different densities, as shown in Figure 9. As in the case of liquid–solid transition, we correct for finite-size effects in the values of the free energy at some fixed density by using different system sizes (i.e., $N = 432$, $N = 1024$, $N = 1296$, and $N = 1458$) and extrapolation (see Figure 10). The parameter λ_{max} in eq 5 is chosen to be 12000 to suppress particle collisions. For each system, 40000 MC cycles are used to equilibrate the system and another 40000 cycles are used to collect the ensemble averaged value of $U(\lambda)$ at each integration point. A common tangent construction is then employed to identify the coexistence densities for the first-order CT to

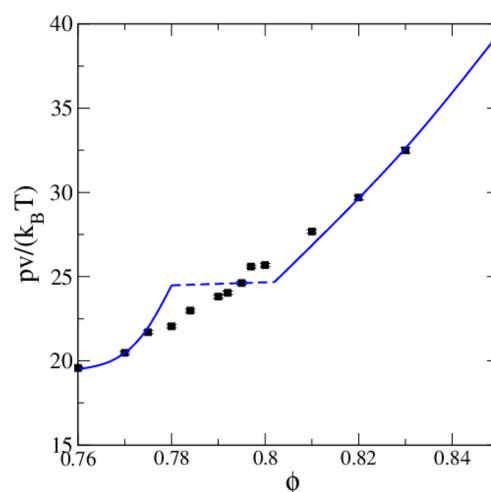


Figure 8. Reduced pressure $pv/(k_B T)$ as a function of packing fraction ϕ at high densities for truncated tetrahedra, where v is the volume of a truncated tetrahedron. The square dots are the actual simulation data and the solid curves are fits of the data for the CT and densest known crystal phases, respectively. The horizontal dash line denotes the coexistence region between these two crystals, which is determined by subsequent free energy calculations. Note that approximately between $\phi \approx 0.775 \pm 0.005$ and $\phi \approx 0.800 \pm 0.002$ the trend for simulation data exhibits discontinuities, suggesting the occurrence of a solid–solid phase transition.

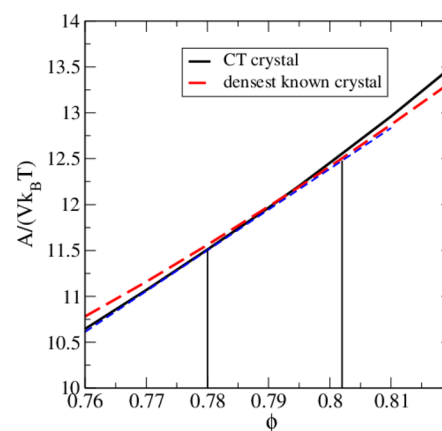


Figure 9. Reduced Helmholtz free energy per unit volume $A/(Vk_B T)$ as a function of packing fraction ϕ for CT crystal phase and densest known crystal phase of hard truncated tetrahedra. The coexistence densities of CT crystal and densest known crystal are estimated to be $\phi = 0.780 \pm 0.002$ and $\phi = 0.802 \pm 0.003$.

densest-known crystal transition, i.e., $\phi \in [0.780 \pm 0.002, 0.802 \pm 0.003]$.

V. MAXIMALLY RANDOM JAMMED PACKINGS OF TRUNCATED TETRAHEDRA

As indicated in section I, a hard-particle system falls out of equilibrium when compressed sufficiently fast to a disordered jammed packing state. The largest possible compression rate consistent with jamming will result in the maximally random jammed packing state. In this section, we generate the MRJ packings of truncated tetrahedra using ASC simulations with a sufficiently large compression rate and then study their structural characteristics.

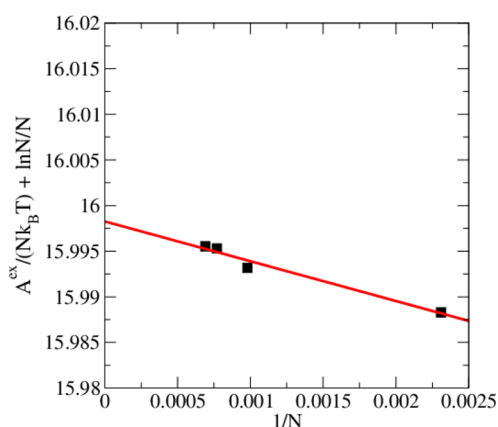


Figure 10. Quantity $A^{\text{ex}}/(Nk_B T) + \ln N/N$ as a function of $1/N$ for a system of truncated tetrahedra in a CT packing crystal at a packing fraction of 0.78, where $A^{\text{ex}} \equiv A - A_{\text{id}}$ is the excess free energy (A_{id} is the ideal gas free energy). The intercept of the ordinate obtained from the linear extrapolation yields the infinite-volume limit of the excess free energy.

A. Generation of MRJ Packings via Fast Compression Using the ASC Scheme. Starting from an unjammed initial packing configuration, the particles are randomly displaced and rotated sequentially. If a trial move (e.g., random displacement or rotation of a particle) causes overlap between a pair of particles, it is rejected; otherwise, the trial move is accepted and a new packing configuration is obtained. After a prescribed number of particle trial moves, small random deformations and compressions/dilations of the simulation box are applied such that the system is on average compressed. The compression rate Γ is defined as the inverse of the number of particle trial moves per particle per simulation-box trial move. For large Γ , the system cannot be sufficiently equilibrated after each compression and will eventually jam with a disordered configuration at a lower density than that of the corresponding maximally dense crystalline packing.¹⁵

Two types of unjammed packings are used as initial configurations: dilute equilibrium hard polyhedron fluids with $\phi < 0.1$ and packings derived from MRJ hard-sphere packings. In the later case, the largest possible polyhedron with random orientation is inscribed into each sphere, which is employed to maximize both translational and orientational disorder in the initial packings. Initial configurations of both types are quickly compressed ($\Gamma \in [0.01, 0.1]$) to maximize disorder until the average interparticle gap is ~ 0.1 of the circumradius of the polyhedra. Then a much slower compression ($\Gamma \in [0.0002, 0.001]$) is used to allow true contact network to be established which induces jamming. The final packings are verified to be strictly jammed by shrinking the particles by a small amount (< 0.01 circumradius) and “equilibrating” the system with a deformable boundary. If there is no increase of the interparticle gaps (decreasing pressure) for a sufficiently long period of time ($> 50\,000$ MC moves per particle), the original packing is considered to be jammed.¹⁵ Translational and orientational order are explicitly quantified by evaluating corresponding correlation functions, which then enables us to find those configurations with a minimal degree of order among a representative set of configurations. This analysis leads to reasonably close approximations to the MRJ states.¹⁵

For truncated tetrahedra, jammed final packings with similar ϕ and structural characteristics can be obtained from both types

of initial configurations. Although larger Γ than employed here can lead to final packings with even lower ϕ and a higher degree of disorder, such packings are generally not jammed, i.e., they are “melt” upon small shrinkage and equilibration. We have used the largest possible initial compression rates ($\Gamma \in [0.01, 0.1]$) that lead to jammed packings. The packings studied here contain $N = 500$ particles. We find that the average packing fraction of the MRJ state of truncated tetrahedra is $\phi_{\text{MRJ}} = 0.770 \pm 0.001$. A representative MRJ packing is shown in Figure 11. Figure 12 schematically depicts the pressure of the

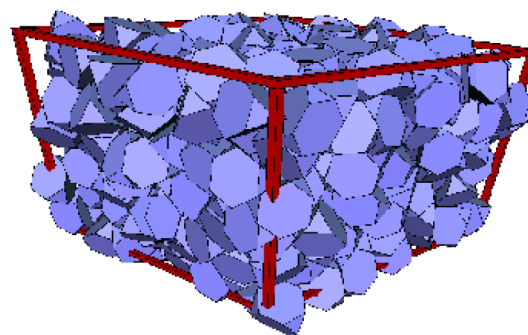


Figure 11. Representative MRJ packing of truncated tetrahedra with $N = 500$ particles.

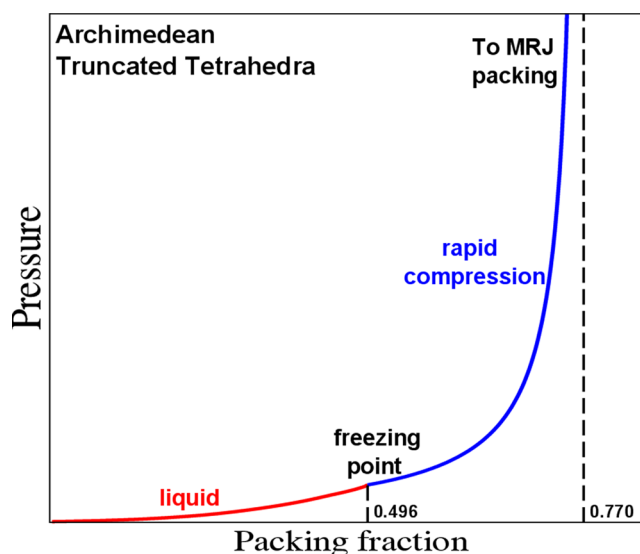


Figure 12. Schematic plot of the pressure of the hard truncated tetrahedra system as a function of packing fraction along the liquid branch and then along a metastable extension of the liquid branch that ends at the MRJ state. Note that the pressure diverges at the jamming point $\phi \approx 0.770$, which is substantially larger than for spheres ($\phi_{\text{MRJ}} \approx 0.64$); see Figure 1.

hard truncated tetrahedra system as a function of packing fraction. Note that the pressure diverges at the jamming point $\phi \approx 0.770$, which is substantially larger than for spheres ($\phi_{\text{MRJ}} \approx 0.64$); see Figure 1.

B. Pair Correlations in MRJ Packings of Truncated Tetrahedra. We find the packing fraction of the MRJ states of truncated tetrahedra is $\phi = 0.770 \pm 0.001$. A representative packing configuration is shown in Figure 11. The panels of Figure 13 show the pair correlation function $g_2(r)$ associated with the particle centroids and the orientational pair correlation function $g_{\text{orient}}(r)$ obtained by averaging over 5 configurations. It

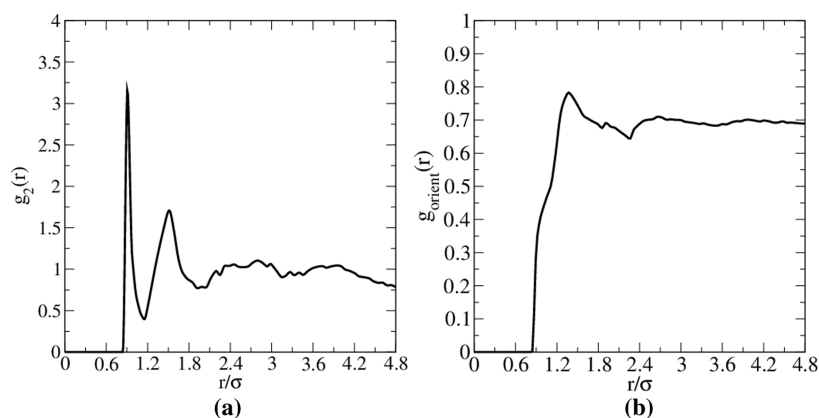


Figure 13. Pair correlation functions versus the dimensionless distance r/σ (where $\sigma = v^{1/3}$) for MRJ packings of truncated tetrahedra obtained by averaging over 5 configurations: (a) centroidal pair correlation function $g_2(r)$ and (b) orientational pair correlation function $g_{\text{orient}}(r)$.

can be seen that $g_2(r)$ possesses several prominent oscillations. However, the magnitude of these oscillations are much smaller than that associated with MRJ packings of hard spheres, or other polyhedra with small asphericity values (e.g., icosahedra). This is because in MRJ sphere packings, the pair distances between contacting neighbors are exactly equal to the diameter of the spheres. However, for nonspherical particles, the pair distances between contacting neighbors in the associated MRJ packings can vary from the diameter of their insphere to that of their circumsphere, and thus, causing large fluctuations of pair distances between the particle centroids. This further diminishes the magnitude of the oscillations in the associated $g_2(r)$, and thus the translational order in the system. The orientational correlation function $g_{\text{orient}}(r)$ also suggests that the packing is orientationally disordered.

Figure 14 shows the structure factor $S(k)$ versus wavenumber k as obtained by averaging over 5 configurations of MRJ

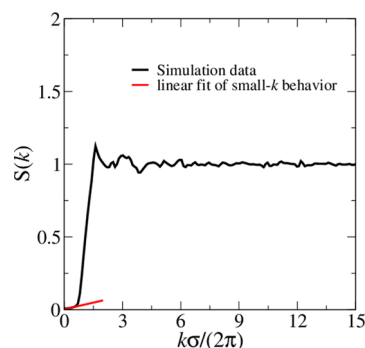


Figure 14. Structure factor $S(k)$ as a function of the dimensionless wavenumber $k\sigma/(2\pi)$ obtained by averaging over five configurations of MRJ packings of truncated tetrahedra, where $\sigma = v^{1/3}$. The red line is a linear fit to the data for small wavenumbers.

packings of truncated tetrahedra. Importantly, we find that $S(k) \rightarrow 0$ as $k \rightarrow 0$, which means they are hyperuniform with quasi-long-range pair correlations (see section III.C). We employ a linear polynomial to approximate the small- k behavior of $S(k)$, i.e., $S(k) = a_0 + a_1 k\sigma/(2\pi)$, and use it to fit computed $S(k)$ and find that $a_0 \approx 0$ ($< 10^{-5}$). Moreover, the slope is $a_1 = 0.030$, which is significantly larger than a_0 . These observations indicate that the MRJ truncated tetrahedron packings possess hyperuniform quasi-long-range (QLR) pair correlations in which $h(r)$ decays asymptotically with scaling $-r^{-4}$, consistent

with our previous studies of MRJ packings of the nontiling Platonic solids. This also provides further evidence that the hyperuniform QLR correlations are a universal signature of MRJ packings of hard convex particles of general shape.⁵⁶ Note that although we are employing a relatively small system with $N = 500$ particles, based on previous research¹⁵ we expect that the extrapolated small- k behavior of $S(k)$ obtained from such systems should agree with extrapolations from large systems. Therefore, our conclusions that MRJ packings of truncated tetrahedra are hyperuniform, based on the relatively small systems that we have studied, should be firm.

It is interesting to compare the slope a_1 of $S(k)$ for small k of truncated tetrahedra to those of other polyhedra that we have previously studied. For icosahedra, dodecahedra, octahedra and tetrahedra, the values of a_1 are respectively 0.015, 0.023, 0.029, and 0.21. It is apparent that as the polyhedral shape deviates more from that of a sphere, the value of the slope a_1 increases, i.e., the degree of hyperuniformity decreases. This is because larger asphericities induce larger local number density fluctuations at fixed long wavelengths (i.e., small k values) due to the QLR correlations.

We would like to note that for nonspherical particles, the more appropriate measure of hyperuniformity is based on local volume fraction fluctuations (rather than density fluctuations) and the small-wavenumber behavior of the associated spectrum density.⁵⁶ Similar conclusions on hyperuniform QLR correlations in the system will be obtained if the more general procedure is used, but with this procedure, the degree of hyperuniformity would decrease with decreasing packing fraction (instead of with increasing asphericity). This is because denser packings possess more homogeneous void spaces, which lead to smaller local volume fraction fluctuations.⁵⁶

Table 2 lists the values of the MRJ packing fraction ϕ_{MRJ} and the packing fraction of the densest known packing ϕ_{max} for different particle shapes.^{10,14,15,17,18,64–70} It is interesting to note that the ratio $\beta = \phi_{\text{MRJ}}/\phi_{\text{max}}$ provides a measure of the extent to which the system is a good glass former. Specifically, when β is close to unity, high-density disordered packings are entropically favored, i.e., it is more difficult to produce the crystal phase and the associated maximally dense packing via simulation or experimental protocols. Indeed, for spheroids with $\beta = 0.95$, the densest-known packing was extremely difficult to obtain via simulations, which requires very slow compression of a small system with a few particles in a fundamental cell with a specific shape.⁶⁵ It has recently been

Table 2. Relationship between the MRJ Packing Fraction ϕ_{MRJ} and the Densest Packing Fraction ϕ_{max} for Congruent Particles of Different Shapes^{a,10,14,15,17,18,64–72}

particle shape	ϕ_{MRJ}	ϕ_{max}	$\phi_{\text{MRJ}}/\phi_{\text{max}}$
octahedron	0.697	0.947	0.736
tetrahedron	0.763	0.856	0.891
dodecahedron	0.716	0.904	0.792
icosahedron	0.707	0.836	0.846
truncated tetrahedron	0.770	0.995	0.774
sphere	0.637	0.741	0.86
prolate spheroid with $b/a = 2$	0.70	0.77	0.91
prolate spheroid with $b/a = 3/2$	0.71	0.75	0.95
oblate spheroid with $b/a = 1/2$	0.70	0.77	0.91
oblate spheroid with $b/a = 2/3$	0.71	0.75	0.95
superball with $q = 0.8$	0.66	0.72	0.92
superball with $q = 1.2$	0.68	0.77	0.88
superball with $q = 2$	0.74	0.86	0.86

^aIn the case of spheroids, b/a is the aspect ratio and in the case of superballs, q is the deformation parameter (where $q = 1$ corresponds to a sphere). A ratio $\phi_{\text{MRJ}}/\phi_{\text{max}}$ close to unity indicates a system that is a good glass former, as discussed in the text.

shown that disordered binary sphere packings can attain MRJ packing densities that are nearly as dense as the densest known packings and therefore are good glass formers.⁷³ Finally, consistent with the results for MRJ packings of nontiling Platonic solids,¹⁵ we find that the rattler-free jammed "backbones"⁷⁴ MRJ packings of truncated tetrahedra are also isostatic (the total number of constraints, related to the different types of interparticle contacts, equals the total number of degrees of freedom in the packing). Specifically, each particle in MRJ packings of truncated tetrahedra has 12.01 contacts on average (the number of face-to-face, edge-to-face, vertex-to-face, and edge-to-edge contact is determined to be 2.79 ± 0.02 , 0.32 ± 0.02 , 0.92 ± 0.02 and 2.07 ± 0.02 , respectively), which is consistent with isostaticity.

VI. CONCLUSIONS AND DISCUSSION

In this paper, we have ascertained the equilibrium phase behavior of truncated tetrahedra over the entire range of possible densities, via ASC Monte Carlo simulations and free energy calculations. We found that the system undergoes first-order liquid–solid and solid–solid phase transitions as the density increases, consistent with the finding in the qualitative study by Jiao and Torquato.¹⁰ The liquid phase coexists with the CT crystal phase within the density range $\phi \in [0.496 \pm 0.006, 0.591 \pm 0.005]$ and the CT phase coexist with the densest-known crystal within the density range $\phi \in [0.780 \pm 0.002, 0.802 \pm 0.003]$. We found no evidence for any stable rotator or nematic phases. We also generated the maximally random jammed (MRJ) packings of truncated tetrahedra, which may be regarded to be the ending state of a metastable branch of the phase diagram for truncated tetrahedra. Specifically, we systematically studied the structural characteristics of the MRJ packings, including the centroidal pair correlation function, structure factor and orientational pair correlation function. We found that such MRJ packings are hyperuniform with an average packing fraction of 0.770 ± 0.001 , which is considerably larger than the corresponding value for identical spheres. We have also shown that the ratio $\phi_{\text{MRJ}}/\phi_{\text{max}}$ for a general nonspherical particle shape provides a measure of its glass-forming ability.

The transition from the CT to the densest-known crystal phase involves symmetry breaking as one would expect. Specifically, the CT packing possess a higher degree of symmetry (rhombohedral) than that of the densest known packing (triclinic). Similar symmetry-breaking crystal–crystal phase transitions have also been observed in systems of truncated cubes with a small degree of truncation,¹² which possess a first-order transition from the simple-cubic phase (with cubic symmetry) to the one associated with the densest-known packing (with rhombohedral symmetry). We conjecture that particles with shapes close to the space-filling ones and that nearly fill all of space (i.e., those obtained by chopping of the corners of rhombohedron, cube, truncated octahedron, and certain prisms) would probably undergo a first-order crystal–crystal transition from a high-symmetry solid phase to a low-symmetry one. The high-symmetry phase should be associated with the optimal configuration of the corresponding space-filling shape, and the low-symmetry phase should be associated with the densest-known packing of the actual particle that is nearly space-filling.^{10,43} Since the low-symmetry phase should possess more free volume and thus is more favorable entropically compared to the high-symmetry phase, we expect that a solid–solid phase transition would occur at high densities in such systems. However, we emphasize that such qualitative predictions about the class of particle shapes that possess crystal–crystal phase transitions has yet to be identified and verified by rigorous free energy calculations.

These results also point to the great challenges in identifying solid–solid phase transitions in hard-particle systems. In particular, for truncated tetrahedra, if one had not known *a priori* about the existence of both crystal structures (i.e., the CT and densest known packings),^{10,43} one would never have tried to see if the phases associated with these distinct crystals could coexist. For example, if one only knew about the densest known packing but not the CT packing, and simply decompressed the packing from the highest density, one likely would have thought there was no other crystal phase. Similarly, if one only knew about CT packing, then further compression of the CT from the melting point would probably not have alerted one to consider another crystal structure at very high densities. This also calls into the question whether in previous studies similar solid–solid phase transitions were missed for other particle shapes because no systematic structural probes were used to ascertain whether the crystal structure changed symmetry. We believe that crystal structures with distinct symmetries should be explicitly examined in order to correctly identify possible solid–solid phase transitions.

It is also useful to compare the phase behavior of truncated tetrahedra to that of other nonspherical shapes, especially the nature of the disorder–order phase transition. Truncated tetrahedra behave like regular octahedra⁹ in that both systems undergo a first-order transition from the isotropic liquid to a crystal phase. It is clear that this transition, which is entropy-driven,⁷⁵ is determined by the characteristics of the particle shape. Both the truncated tetrahedron and regular octahedron have an aspect ratio δ (defined to be the ratio between the longest and shortest principal axis) of unity. They also possess moderately sized values of a relative scaled exclusion volume $\tau \equiv v_{\text{ex}}/(8v)$,⁴² i.e., $\tau = 1.236$ and 1.330 for truncated tetrahedra and octahedra, respectively. Upon forming the crystal phase from the liquid, a sufficiently large increase of free-volume entropy is achieved by particle alignment and positional ordering, and thus, the crystal phase is favored. For shapes

close to that of a sphere, such as ellipsoids with small δ and superballs with τ close to unity, the associated systems possess a transition from isotropic to rotator phase. This is because orientational ordering does not lead to significant increase of free-volume entropy, and thus, is not favored. On the other hand, as the aspect ratio of an ellipsoid increases beyond a critical value (e.g., $\delta > 2$), the systems start to form a nematic phase from liquid upon compression,⁷ due to a large gain of free-volume entropy by particle alignment.

On the basis of the aforementioned observations and other previous research,^{7,9,10,12} we predict the phase that breaks the symmetry of the liquid for systems of hard nonspherical particles such as the regular icosahedra, dodecahedra,⁷⁶ and rectangular parallelepiped (with side lengths a , b , and c , and $a \neq b \neq c$). Specifically, we expect that when the relative scaled exclusion volume τ for particles with flat faces is less than the order of 1.2, it is highly possible that rotator phase arises upon compression from isotropic liquid phase. The scaled exclusion volume of icosahedron is given by $v_{ex}/v = [2 + (90\sqrt{3} \cos^{-1}(\sqrt{5/3})/\pi(2 + \sqrt{5}))] \approx 8.915$,⁴² and the relative scaled exclusion volume is $\tau = 1.114$, which is very close to 1. Therefore, we expect the icosahedron systems to possess an isotropic-rotator phase transition. Similarly, the scaled exclusion volume of dodecahedron is given by $v_{ex}/v = [2 + (90(25 + 10\sqrt{5})^{1/2} \cos^{-1}(1/\sqrt{5})/\pi(15 + 7\sqrt{5}))] \approx 9.121$ and $\tau = 1.140$.⁴² We see again that the later value is close to 1, which suggests that the dodecahedron system is likely to possess a rotator phase upon compression from isotropic liquid phase as well. The scaled exclusion volume of rectangular parallelepiped ($a \neq b \neq c$) is given by $v_{ex}/v = [2 + ((ab + bc + ac)(a + b + c)/abc)]$. Again, when the value of τ is less than the order of 1.2, we expect that there exists a phase transition from the isotropic liquid to a rotator phase. Rigorous free energy calculations will be able to verify such predictions.

AUTHOR INFORMATION

Corresponding Author

*(S.T.) E-mail: torquato@princeton.edu.

Notes

The authors declare no competing financial interest.

ACKNOWLEDGMENTS

We are grateful to Ran Ni for very helpful discussions. This work was supported in part by the National Science Foundation under Grants No. DMR-0820341 and No. DMS-1211087. This work was partially supported by a grant from the Simons Foundation (Grant No. 231015 to S.T.).

REFERENCES

- (1) Frenkel, D.; Smit, B. *Understanding Molecular Simulation: from Algorithms to Applications*; Academic Press: San Diego, CA, and London, 2001.
- (2) Chaikin, P. M.; Lubensky, T. C. *Principles of Condensed Matter Physics*; Cambridge Univ Press: New York, 2000; Vol. 1.
- (3) Zallen, R. *The Physics of Amorphous Solids*; Wiley: New York, 1983.
- (4) Torquato, S. *Random Heterogeneous Materials: Microstructure and Macroscopic Properties*; Springer: New York, 2002; Vol. 16.
- (5) Edwards, S. F. *Granular Matter*; Springer: New York, 1994.
- (6) Zohdi, T. I. A Direct Particle-Based Computational Framework for Electrically Enhanced Thermo-Mechanical Sintering of Powdered Materials. *Math. Mech. Solids* **2014**, *19*, 93–113.

- (7) Bautista-Carbajal, G.; Moncho-Jordá, A.; Odriozola, G. Further Details on the Phase Diagram of Hard Ellipsoids of Revolution. *J. Chem. Phys.* **2013**, *138*, 064501.
- (8) Frenkel, D.; Mulder, B. M.; Mctague, J. P. Phase Diagram of Hard Ellipsoids of Revolution. *Mol. Cryst. Liq. Cryst.* **1985**, *123*, 119–128.
- (9) Ni, R.; Gantapara, A. P.; de Graaf, J.; van Roij, R.; Dijkstra, M. Phase Diagram of Colloidal Hard Superballs: from Cubes via Spheres to Octahedra. *Soft Matter* **2012**, *8*, 8826–8834.
- (10) Jiao, Y.; Torquato, S. Communication: A Packing of Truncated Tetrahedra that Nearly Fills All of Space and its Melting Properties. *J. Chem. Phys.* **2011**, *135*, 151101.
- (11) Vega, C.; Sanz, E.; Abascal, J.; Noya, E. Determination of Phase Diagrams via Computer Simulation: Methodology and Applications to Water, Electrolytes and Proteins. *J. Phys.: Condens. Mat.* **2008**, *20*, 153101.
- (12) Gantapara, A. P.; de Graaf, J.; van Roij, R.; Dijkstra, M. Phase Diagram and Structural Diversity of a Family of Truncated Cubes: Degenerate Close-Packed Structures and Vacancy-Rich States. *Phys. Rev. Lett.* **2013**, *111*, 015501.
- (13) Donev, A.; Cisse, I.; Sachs, D.; Variano, E. A.; Stillinger, F. H.; Connelly, R.; Torquato, S.; Chaikin, P. M. Improving the Density of Jammed Disordered Packings Using Ellipsoids. *Science* **2004**, *303*, 990–993.
- (14) Jiao, Y.; Stillinger, F. H.; Torquato, S. Distinctive Features Arising in Maximally Random Jammed Packings of Superballs. *Phys. Rev. E* **2010**, *81*, 041304.
- (15) Jiao, Y.; Torquato, S. Maximally Random Jammed Packings of Platonic Solids: Hyperuniform Long-Range Correlations and Isostaticity. *Phys. Rev. E* **2011**, *84*, 041309.
- (16) Agarwal, U.; Escobedo, F. A. Mesophase Behaviour of Polyhedral Particles. *Nat. Mater.* **2011**, *10*, 230–235.
- (17) Torquato, S.; Jiao, Y. Dense Packings of the Platonic and Archimedean Solids. *Nature* **2009**, *460*, 876–879.
- (18) Torquato, S.; Jiao, Y. Dense Packings of Polyhedra: Platonic and Archimedean Solids. *Phys. Rev. E* **2009**, *80*, 041104.
- (19) Neudecker, M.; Ulrich, S.; Herminghaus, S.; Schröter, M. Jammed Frictional Tetrahedra are Hyperstatic. *Phys. Rev. Lett.* **2013**, *111*, 028001.
- (20) Xia, X.; Xia, Y. Symmetry Breaking during Seeded Growth of Nanocrystals. *Nano Lett.* **2012**, *12*, 6038–6042.
- (21) Rossi, L.; Sacanna, S.; Irvine, W. T.; Chaikin, P. M.; Pine, D. J.; Philipse, A. P. Cubic Crystals from Cubic Colloids. *Soft Matter* **2011**, *7*, 4139–4142.
- (22) Quan, Z.; Fang, J. Superlattices with Non-Spherical Building Blocks. *Nano Today* **2010**, *5*, 390–411.
- (23) Schweiger, M.; Yamamoto, T.; Stang, P. J.; Bläser, D.; Boese, R. Self-Assembly of Nanoscale Supramolecular Truncated Tetrahedra. *J. Org. Chem.* **2005**, *70*, 4861–4864.
- (24) Torquato, S.; Truskett, T. M.; Debenedetti, P. G. Is Random Close Packing of Spheres Well Defined? *Phys. Rev. Lett.* **2000**, *84*, 2064.
- (25) Torquato, S.; Stillinger, F. H. Jammed Hard-Particle Packings: From Kepler to Bernal and Beyond. *Rev. Mod. Phys.* **2010**, *82*, 2633.
- (26) Alder, B. J.; Wainwright, T. E. Phase Transition for a Hard Sphere System. *J. Chem. Phys.* **1957**, *27*, 1208.
- (27) Hansen, J. P.; Macdonald, I. R. *Theory of Simple Liquids*; Academic Press: London, 1986.
- (28) Frenkel, D.; Ladd, A. J. New Monte Carlo Method to Compute the Free Energy of Arbitrary Solids. Application to the fcc and hcp Phases of Hard Spheres. *J. Chem. Phys.* **1984**, *81*, 3188.
- (29) Rintoul, M. D.; Torquato, S. Computer Simulations of Dense Hard-Sphere Systems. *J. Chem. Phys.* **1996**, *105*, 9258.
- (30) Speedy, R. J. Pressure and Entropy of Hard-Sphere Crystals. *J. Phys.: Condens. Mat.* **1998**, *10*, 4387–4391.
- (31) Mau, S. C.; Huse, D. A. Stacking Entropy of Hard-Sphere Crystals. *Phys. Rev. E* **1999**, *59*, 4396.
- (32) Jadrlich, R.; Schweizer, K. S. Equilibrium Theory of the Hard Sphere Fluid and Glasses in the Metastable Regime up to Jamming. I. Thermodynamics. *J. Chem. Phys.* **2013**, *139*, 054501.

- (33) Jadrlich, R.; Schweizer, K. S. Equilibrium Theory of the Hard Sphere Fluid and Glasses in the Metastable Regime up to Jamming. II. Structure and Application to Hopping Dynamics. *J. Chem. Phys.* **2013**, *139*, 054502.
- (34) Vega, C.; Monson, P. Solid-Liquid Equilibrium for a Molecular Model with Short Ranged Directional Forces. *J. Chem. Phys.* **1998**, *109*, 9938.
- (35) Bolhuis, P. G.; Frenkel, D.; Mau, S.-C.; Huse, D. A. Entropy Difference between Crystal Phases. *Nature* **1997**, *388*, 235–236.
- (36) Marechal, M.; Kortschot, R. J.; Demirörs, A. F.; Imhof, A.; Dijkstra, M. Phase Behavior and Structure of a New Colloidal Model System of Bowl-Shaped Particles. *Nano Lett.* **2010**, *10*, 1907–1911.
- (37) Onsager, L. The Effects of Shape on the Interaction of Colloidal Particles. *Ann. N.Y. Acad. Sci.* **1949**, *51*, 627–659.
- (38) Rego, J. A.; Harvey, J. A.; MacKinnon, A. L.; Gatdula, E. Asymmetric Synthesis of a Highly Soluble ‘Trimeric’ Analogue of the Chiral Nematic Liquid Crystal Twist Agent Merck S1011. *Liq. Cryst.* **2009**, *37*, 37–43.
- (39) Frenkel, D.; Lekkerkerker, H. N. W.; Stroobants, A. Thermodynamic Stability of a Smectic Phase in a System of Hard Rods. *Nature* **1988**, *332*, 822–823.
- (40) Batten, R. D.; Stillinger, F. H.; Torquato, S. Phase Behavior of Colloidal Superballs: Shape Interpolation from Spheres to Cubes. *Phys. Rev. E* **2010**, *81*, 061105.
- (41) Carbone, P.; Avendaño, C. Coarse-Grained Methods for Polymeric Materials: Enthalpy- and Entropy-Driven Models. *WIREs Comput. Mol. Sci.* **2014**, *4*, 62–70.
- (42) Torquato, S.; Jiao, Y. Effect of Dimensionality on the Percolation Thresholds of Overlapping Nonspherical Hyperparticles. *Phys. Rev. E* **2013**, *87*, 022111.
- (43) Conway, J. H.; Torquato, S. Packing, Tiling, and Covering with Tetrahedra. *Proc. Natl. Acad. Sci. U.S.A.* **2006**, *103*, 10612–10617.
- (44) Torquato, S.; Stillinger, F. H. Local Density Fluctuations, Hyperuniform Systems, and Order Metrics. *Phys. Rev. E* **2003**, *68*, 041113.
- (45) Golshtein, E. G. *Modified Lagrangians and Monotone Maps in Optimization*; Wiley: New York, 1996; Vol. 30.
- (46) Eppenga, R.; Frenkel, D. Monte Carlo Study of the Isotropic and Nematic Phases of Infinitely Thin Hard Platelets. *Mol. Phys.* **1984**, *52*, 1303–1334.
- (47) Widom, B. Some Topics in the Theory of Fluids. *J. Chem. Phys.* **1963**, *39*, 2808–2812.
- (48) Noya, E. G.; Conde, M.; Vega, C. Computing the Free Energy of Molecular Solids by the Einstein Molecule Approach: Ices XIII and XIV, Hard-Dumbbells and a Patchy Model of Proteins. *J. Chem. Phys.* **2008**, *129*, 104704.
- (49) Gray, C.; Gubbins, K. *Theory of Molecular Fluids*; Clarendon: Oxford, 1984.
- (50) Noya, E. G.; Vega, C.; Doye, J. P. K.; Louis, A. A. The stability of a Crystal with Diamond Structure for Patchy Particles with Tetrahedral Symmetry. *J. Chem. Phys.* **2010**, *132*, 234511.
- (51) A Kepler-like conjecture for certain centrally symmetric polyhedra¹⁷ purports that the densest packing of regular octahedra is the densest Bravais lattice packing of such objects first found by Minkowski.⁵²
- (52) Minkowski, H. Dichteste Gitterförmige Lagerung Kongruenter Körper. *Nachr. Ges. Wiss. Göttingen, Math.-Phys. Kl.* **1904**, 311–355.
- (53) Zachary, C. E.; Torquato, S. Hyperuniformity in Point Patterns and Two-Phase Random Heterogeneous Media. *J. Stat. Mech. Theor. Exp.* **2009**, P12015.
- (54) Torquato, S.; Scardicchio, A.; Zachary, C. E. Point Processes in Arbitrary Dimension from Fermionic Gases, Random Matrix Theory, and Number Theory. *J. Stat. Mech. Theor. Exp.* **2008**, P11019.
- (55) Batten, R. D.; Stillinger, F. H.; Torquato, S. Classical Disordered Ground States: Super-Ideal Gases, and Stealth and Equi-Luminous Materials. *J. Appl. Phys.* **2008**, *104*, 033504.
- (56) Zachary, C. E.; Jiao, Y.; Torquato, S. Hyperuniform Long-Range Correlations are a Signature of Disordered Jammed Hard-Particle Packings. *Phys. Rev. Lett.* **2011**, *106*, 178001.
- (57) Zachary, C. E.; Torquato, S. Anomalous Local Coordination, Density Fluctuations, and Void Statistics in Disordered Hyperuniform Many-Particle Ground States. *Phys. Rev. E* **2011**, *83*, 051133.
- (58) Zachary, C. E.; Jiao, Y.; Torquato, S. Hyperuniformity, Quasi-Long-Range Correlations, and Void Space Constraints in Maximally Random Jammed Particle Packings. I. Polydisperse Spheres. *Phys. Rev. E* **2011**, *83*, 051308.
- (59) Zachary, C. E.; Jiao, Y.; Torquato, S. Hyperuniformity, Quasi-Long-Range Correlations, and Void Space Constraints in Maximally Random Jammed Particle Packings. II. Anisotropy in Particle Shape. *Phys. Rev. E* **2011**, *83*, 051309.
- (60) Florescu, M.; Torquato, S.; Steinhardt, P. J. Designer Disordered Materials with Large, Complete Photonic Band Gaps. *Proc. Natl. Acad. Sci. U.S.A.* **2009**, *106*, 20658–20663.
- (61) Jiao, Y.; Lau, T.; Hatzikirou, H.; Meyer-Hermann, M.; Corbo, J. C.; Torquato, S. Avian Photoreceptor Patterns Represent a Disordered Hyperuniform Solution to a Multiscale Packing Problem. *Phys. Rev. E* **2014**, *89*, 022721.
- (62) Boublik, T. Equation of State of Hard Convex Body Fluids. *Mol. Phys.* **1981**, *42*, 209–216.
- (63) Polson, J.; Trizac, E.; Pronk, S.; Frenkel, D. Finite-Size Corrections to the Free Energies of Crystalline Solids. *J. Chem. Phys.* **2000**, *112*, 5339–5342.
- (64) Jiao, Y.; Stillinger, F. H.; Torquato, S. Optimal Packings of Superballs. *Phys. Rev. E* **2009**, *79*, 041309.
- (65) Donev, A.; Stillinger, F. H.; Chaikin, P. M.; Torquato, S. Unusually Dense Crystal Ellipsoid Packings. *Phys. Rev. Lett.* **2004**, *92*, 255506.
- (66) Chaikin, P. M.; Donev, A.; Man, W.; Stillinger, F. H.; Torquato, S. Some Observations on the Random Packing of Hard Ellipsoids. *Ind. Eng. Chem. Res.* **2006**, *45*, 6960–6965.
- (67) Hales, T. C. A Proof of the Kepler Conjecture. *Ann. Math.* **2005**, *162*, 1065–1185.
- (68) Torquato, S.; Stillinger, F. H. Multiplicity of Generation, Selection, and Classification Procedures for Jammed Hard-Particle Packings. *J. Phys. Chem. B* **2001**, *105*, 11849.
- (69) Kansal, A. R.; Torquato, S.; Stillinger, F. H. Diversity of Order and Densities in Jammed Hard-Particle Packings. *Phys. Rev. E* **2002**, *66*, 041109.
- (70) Torquato, S.; Jiao, Y. Exact Constructions of a Family of Dense Periodic Packings of Tetrahedra. *Phys. Rev. E* **2010**, *81*, 041310.
- (71) Kallus, Y.; Elser, S.; Gravel, V. Dense Periodic Packings of Tetrahedra with Small Repeating Units. *Discrete Comput. Geom.* **2010**, *44*, 245–252.
- (72) Chen, E. R.; Engel, M.; Glotzer, S. C. Dense Crystalline Dimer Packings of Regular Tetrahedra. *Discrete Comput. Geom.* **2010**, *44*, 253–280.
- (73) Hopkins, A. B.; Stillinger, F. H.; Torquato, S. Disordered Strictly Jammed Binary Sphere Packings Attain an Anomously Large Range of Densities. *Phys. Rev. E* **2013**, *88*, 022205.
- (74) Atkinson, S.; Stillinger, F. H.; Torquato, S. Detailed Characterization of Rattlers in Exactly Isostatic, Strictly Jammed Sphere Packings. *Phys. Rev. E* **2013**, *88*, 062208.
- (75) Frenkel, D. Entropy-Driven Phase Transitions. *Physica A* **1999**, *263*, 26–38.
- (76) We note that such rotator phases were observed in Monte-Carlo simulations.⁷⁷ However, rigorous free energy calculations are still required to verify that these phases are thermodynamically stable rather than metastable.
- (77) Damasceno, P. F.; Engel, M.; Glotzer, S. C. Predictive Self-Assembly of Polyhedra into Complex Structures. *Science* **2012**, *337*, 453–457.